

Article

# An Extremely Close Vibration Frequency Signal Recognition Using Deep Neural Networks

Mentari Putri Jati <sup>1,2</sup>, Muhammad Irfan Luthfi <sup>3</sup>, Cheng-Kai Yao <sup>1</sup>, Amare Mulatie Dehnaw <sup>1</sup>,  
Yibeltal Chanie Manie <sup>1</sup> and Peng-Chun Peng <sup>1,\*</sup>

<sup>1</sup> Department of Electro-Optical Engineering, National Taipei University of Technology, Taipei 10608, Taiwan; t111999402@ntut.edu.tw or mentariputrihati@uny.ac.id (M.P.J.); t109658093@ntut.org.tw (C.-K.Y.); amare.mulatie@ntut.edu.tw (A.M.D.); yibeltal\_chanie@mail.ntut.edu.tw (Y.C.M.)

<sup>2</sup> Department of Electrical and Electronics Engineering, Vocational Faculty, Universitas Negeri Yogyakarta, Yogyakarta 55281, Indonesia

<sup>3</sup> Department of Electronics and Informatics Engineering Education, Engineering Faculty, Universitas Negeri, Yogyakarta 55281, Indonesia; m.irfanluthfi@uny.ac.id

\* Correspondence: pcpeng@ntut.edu.tw; Tel.: +886-2-2771-2171 (ext. 4671)

**Abstract:** This study proposes the utilization of an optical fiber vibration sensor for detecting the superposition of extremely close frequencies in vibration signals. Integration of deep neural networks (DNN) proves to be meaningful and efficient, eliminating the need for signal analysis methods involving complex mathematical calculations and longer computation times. Simulation results of the proposed model demonstrate the remarkable capability to accurately distinguish frequencies below 1 Hz. This underscores the effectiveness of the proposed image-based vibration signal recognition system embedded in DNN as a streamlined yet highly accurate method for vibration signal detection, applicable across various vibration sensors. Both simulation and experimental evaluations substantiate the practical applicability of this integrated approach, thereby enhancing electric motor vibration monitoring techniques.

**Keywords:** vibration detection; electric motor; deep neural network; Fiber Bragg Grating sensor



**Citation:** Jati, M.P.; Luthfi, M.I.; Yao, C.-K.; Dehnaw, A.M.; Manie, Y.C.; Peng, P.-C. An Extremely Close Vibration Frequency Signal Recognition Using Deep Neural Networks. *Appl. Sci.* **2024**, *14*, 2855. <https://doi.org/10.3390/app14072855>

Academic Editors: Chengjin Qin and Liang Yu

Received: 29 February 2024

Revised: 25 March 2024

Accepted: 26 March 2024

Published: 28 March 2024



**Copyright:** © 2024 by the authors. Licensee MDPI, Basel, Switzerland. This article is an open access article distributed under the terms and conditions of the Creative Commons Attribution (CC BY) license (<https://creativecommons.org/licenses/by/4.0/>).

## 1. Introduction

Electric motors are indispensable for enhancing modern society. These machines play a pivotal role in various applications, such as industrial plants, electric vehicles, renewable energy, agriculture, building infrastructures, etc., contributing significantly to advancing technology and improving overall well-being. As essential components in numerous systems, monitoring vibration signals in electric motors is necessary for understanding machine characteristics and conditions, with a particular emphasis on early-stage fault detection [1–4]. The vibration of motor application in the site plant can be used to identify potential problems with continuous condition monitoring. However, the complexity of motor systems, often comprising multiple motors operating simultaneously and using coupling in motor sets, necessitates advanced methods for detecting vibration signals with high precision.

Detecting vibration signals on critical components of motor systems, encompassing intricate vibration signals, necessitates using multiple sensors to capture comprehensive data. This requirement stems from the specific and variable characteristics inherent in motor vibration signals. Due to the diverse operating conditions and potential fault modes of motors, the vibration signals they produce can exhibit a high degree of specificity and variability. Consequently, employing several sensors enables a more thorough assessment of the vibration patterns, facilitating a comprehensive understanding of the motor's condition and performance.

By capturing data from various points within the motor system, users can better analyze the complex vibration signals and promptly identify anomalies or potential issues. Thus, utilizing multiple sensors enhances the effectiveness of vibration signal detection and contributes to the overall reliability and efficiency of motor systems. Periodically identifying potential problems in motor systems is imperative for ensuring operational reliability and preventing catastrophic failures [5,6].

Figure 1 depicts the monitoring of motor vibrations across different plants, showcasing numerous motors that are essential in large-scale industrial operations. The monitoring process involves capturing motor vibration signals from a distance, typically in office buildings away from the plant site. Employing sophisticated machine learning techniques enables precise identification of the vibration signal frequencies, aiding in the timely detection of potential motor faults.

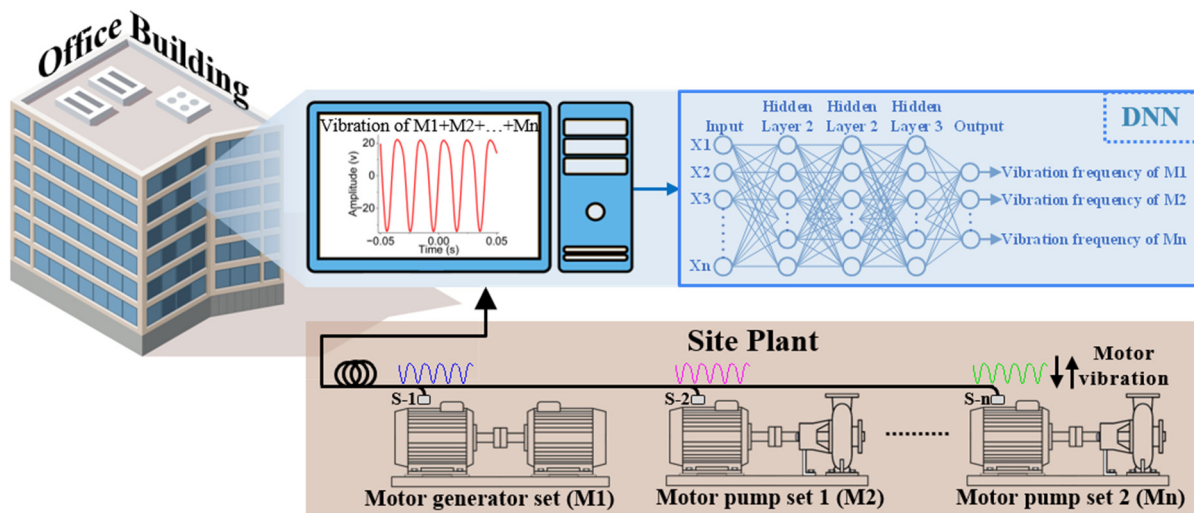


**Figure 1.** The scenario of vibration signal measurement using a DNN approach for electric machines condition monitoring. (DNN: Deep neural networks, M: Motor, S: Sensor).

An accurately recognizing vibration signal frequencies within a specified range poses a considerable dilemma when employing the Fast Fourier Transform (FFT) algorithm as a widely used signal analysis method. The basic FFT is a discretized temporal approximation of the underlying continuous-time mathematical principles. One prominent constraint lies in the implicit assumption of a periodic and stationary signal, which may not accurately represent non-stationary or time-varying signals. Additionally, the discrete nature of the basic FFT introduces spectral leakage [7,8], where energy from one frequency may spread into adjacent frequencies, potentially leading to misinterpretation of spectral content. Moreover, the basic FFT assumes uniformly sampled data, and deviations from this regular sampling may result in artifacts and inaccuracies.

The inherent limitations of the basic FFT become evident as attempts are made to attain such satisfactory resolutions within the given frequency band. Thus, a critical observation arises from realizing that recognizing an extremely close frequency resolution below 1 Hz is vital in motor vibration signal monitoring. This raises challenges regarding computational efficiency and the practicality of acquiring and processing the data required for precise frequency analysis. In Refs. [5,7–11], the basic FFT combines with other methods such as back-propagation neural network, least square method, the hybrid with discrete Fourier transform, prism signal processing, convolutional neural network, and Hilbert transform to overcome its limitations, respectively.

Fiber Bragg Grating (FBG) stands out for vibration sensor applications as a valuable tool for recognizing signal frequencies [12]. To make the sensor more sensitive, the techniques in [13–16] enhance the FBG's structure and utilize a more significant number of FBGs. FBG sensing has been applied in various areas, such as detecting earthquakes, fault

detections, water level monitoring, flowmeter applications, measuring inclinations, health monitoring, and damage location determination [17–23]. The perks of FBG sensors, such as being resistant to electromagnetic interference, small size, and flexibility, make them a promising option for advanced vibration detection. This is especially important in intricate systems with multiple motors, emphasizing FBG's crucial role as a vibration sensor [24,25].

In discerning optical fiber vibration sensing, utilizing Deep Neural Networks (DNN) stands out as a methodology with distinct advantages. Previous investigations into this domain have witnessed the employment of various controllers, including random forest, convolutional neural networks (CNN) + support vector machine (SVM), adaptive filtering CNN, reinforcement learning, SVM, fractional-order PID, YOLO, and XGBoost [11,26–32]. While demonstrating in extremely close frequency scenarios, these controllers have not addressed vibration signal frequency recognition. This gap is urgent due to the importance of accurately detecting such frequencies, particularly in applications like electric motor monitoring and fault detection.

Failure to address this issue may lead to erroneous diagnoses and overlooked anomalies, potentially resulting in costly downtime, equipment damage, or safety hazards. Therefore, there is a pressing need to develop and implement robust controllers that can effectively handle the challenges posed by extremely close frequency scenarios, ensuring reliable and precise vibration signal frequency recognition in engineering systems. Understanding the crucial aspects often overlooked in discussions related to conventional signal analysis and common machine learning approaches, a new novel system is proposed in this study.

The proposed integration of an FBG structure as an optical fiber vibration sensing method for detecting extremely close frequencies in vibration signals from electric motors marks a significant advancement in condition monitoring. The contributions of this study are described as follows:

- To recognize extremely close frequencies of vibration signals without any signal analysis methods often entails intricate mathematical calculations and protracted computation times;
- To demonstrate an efficient and meaningful alternative of the DNN model for accurately recognized vibration signal frequency with a simple FBG configuration system;
- To demonstrate that the proposed system is adaptable to various other types of vibration sensors.

The image-based vibration signal recognition system embedded in DNN holds potential applicability beyond its immediate scope. Furthermore, its versatility extends to detecting and analyzing acoustic signals, broadening its utility across multiple signal processing and analysis domains. This study introduces an innovative perspective in vibration signal analysis by presenting a novel merger of a simple FBG technology and DNN for detecting extremely close frequencies within motor vibrations, an approach hitherto unexplored in the existing literature.

The proposed system configuration is designed to acquire vibration signals with exceptional proximity and high precision, with its underlying concepts drawing inspiration from the diagram block presented in [33]. Furthermore, a deep learning approach is employed to ensure robust precision in vibration measurements, as illustrated in Figure 2. This system configuration is applicable in on-site production plants, energy plants, utility plants, etc., that consist of a lot of vibration from any source. The proposed configuration system consists of a tunable laser (TL) that functions as a broadband source, emitting light through the fiber. The optical circulator (OC) directs the light to the FBG, which is linked to a vibration generator (VG) powered by a signal generator (SG) for precise frequency adjustments. The FBG, sensitive to strain, senses vibration signals corresponding to the frequency set by the SG. The photodetector (PD) captures the vibration signal, which is then directed to the oscilloscope (OSC) for analysis in the time domain.

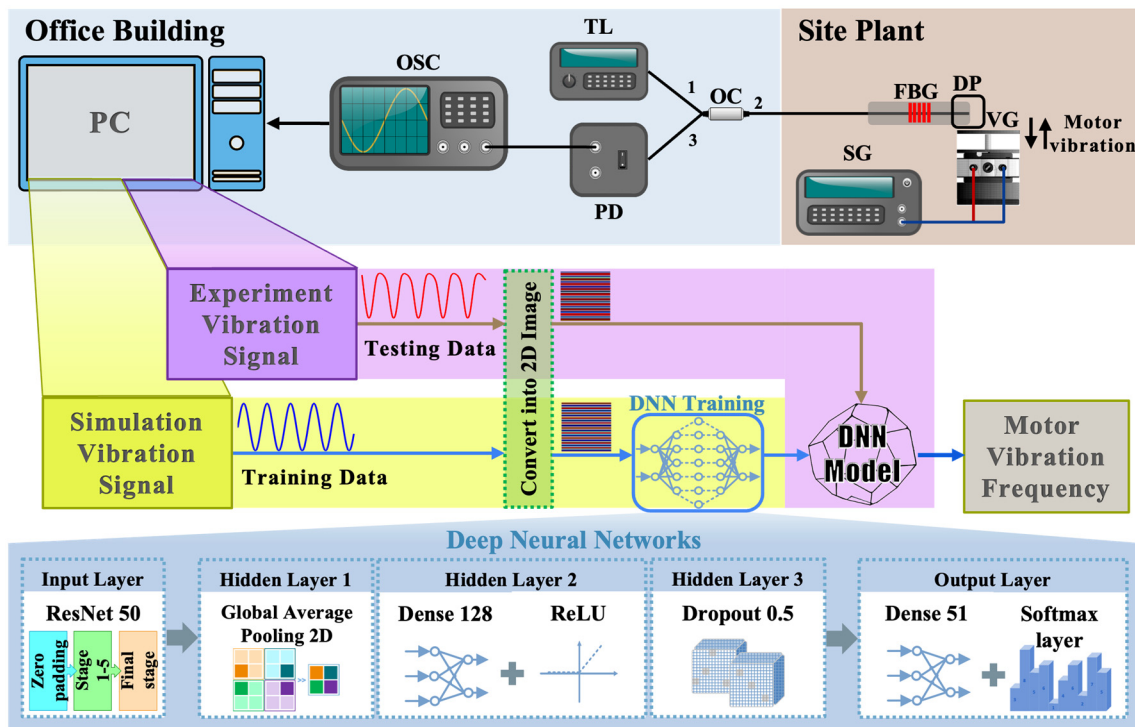


**Figure 2.** The proposed configuration of vibration detection. (PC: Personal computer, OSC: Oscilloscope, TL: Tunable laser, PD: Photodetector, OC: Optical circulator, FBG: Fiber Bragg Grating, DP: Displacement platform, VG: Vibration generator, SG: Signal generator).

The personal computer (PC) analyzes the experimental vibration signal for testing and produces simulation vibration signals for both training and testing purposes. This achievement validates the efficacy of the proposed image-based vibration signal recognition system embedded in DNN and positions it as a precise yet streamlined method for vibration signal detection to identify the frequency of each vibration motor.

Beyond theoretical contributions, the research extends to practical implementation, exemplified by successfully applying the proposed methodology in simulation and specific experimental settings. This dual-validation approach enriches the theoretical framework and establishes the practical viability of the proposed image-based vibration signal recognition system embedded in DNN, offering a more accessible and accurate approach to vibration signal detection in electric motors. Consequently, the study contributes substantially to advancing state-of-the-art condition monitoring and fault detection techniques within electric motor systems.

The remainder of the article is arranged as follows. Section 2 explains the vibration signal recognition using signal analysis methods. Section 3 discusses the proposed image-based vibration signal recognition system embedded in DNN. The results and discussion are validated in Section 4. Finally, the conclusion is provided in Section 5.

## 2. Vibration Signal Detections

In vibration signal detection, sampling frequency and sampling rate differ, particularly when identifying extremely close frequencies. The sampling frequency, representing the number of samples taken within a given time frame, plays a pivotal role in determining the resolution of the frequency content within the signal. Differently, the sampling rate, delineating the number of samples acquired per unit of time, is a critical parameter influencing the accuracy of signal representation. Detailing the response of the signal analysis method for vibration signal detections, we choose an optimal sampling frequency. This research focuses on the vibration signal with various frequencies, fixed amplitude, and phase, and neglecting the signal noise level.

### 2.1. Signal Analysis Methods

#### 2.1.1. Fast Fourier Transform (FFT)

The Fast Fourier Transform (FFT) algorithm emerges as a widely used analysis method to identify signal frequencies, especially vibrational data. The basic FFT algorithm facilitates the transformation of time-domain signals into their frequency-domain counterparts to identify the spectral content within the vibrational data. When detecting close frequencies, the basic FFT can help distinguish between different frequency components present in a signal. The resolution of the basic FFT depends on the number of samples in the input signal and the sampling rate.

More minor differences between vibration signals will result in frequency peaks closer together or look like just a single frequency in the basic FFT output, making distinguishing them more challenging. The equation of the typical vibration signal is given below [5,34].

$$y(t) = \sum_{i=1}^m b_i \cos(2\pi f_i t + \varphi_i) \tag{1}$$

$$\cos(x + y) = \cos x * \cos y - \sin x * \sin y \tag{2}$$

where  $x$  or  $y$  is a signal function,  $m$  is the quantity of frequency,  $f_i$  is the frequency function,  $\varphi_i$  is the phase,  $b_i$  is the amplitude of sine or cosine.

The discrete nature of the basic FFT assumes a periodic and stationary signal, which may not accurately represent the complex dynamics of vibration signals characterized by extremely close frequencies, as shown in Figure 3.

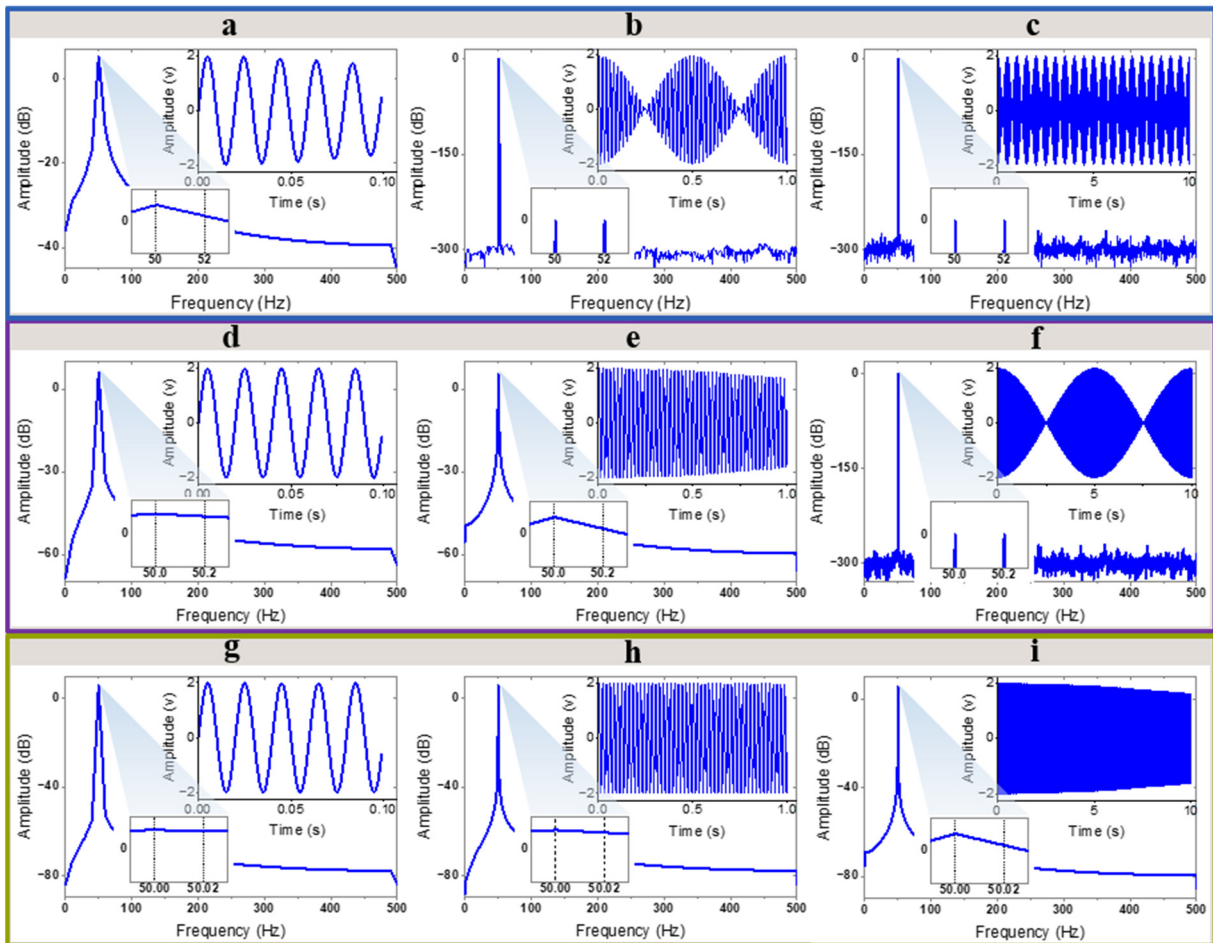


**Figure 3.** Fast Fourier Transform (FFT). (a–c) 50.00 + 52.00 Hz with times 0.1 s, 1 s, 10 s; (d–f) 50.00 + 50.20 Hz with times 0.1 s, 1 s, 10 s; (g–i) 50.00 + 50.02 Hz with times 0.1 s, 1 s, 10 s.

It is imperative to acknowledge the notable drawback of spectral leakage, an artifact that arises due to the fundamental process of basic Fast Fourier Transform (FFT) operations. Spectral leakage can significantly exacerbate the challenge of distinguishing between closely positioned frequency components, thereby complicating accurate analysis and interpretation of data in various applications.

As part of the methodological approach, the study will carefully consider these limitations, addressing them through complementary techniques or alternative signal analysis methods, ensuring a comprehensive understanding of the vibrational data. The vibration signal-based FFT algorithm using sinusoidal waves was tested at various times and superposition frequencies.

The first superposition frequency is 50.00 Hz and 52.00 Hz, shown in Figure 3a, Figure 3b, and Figure 3c, respectively. The second is 50.00 Hz and 50.20 Hz, shown in Figure 3d, Figure 3e, and Figure 3f, respectively. The third is 50.00 Hz and 50.02 Hz, shown in Figure 3g, Figure 3h, and Figure 3i, respectively. All the simulation superposition frequencies use time 0.1 s, 1 s, and 10 s and sampling frequency 1000. The  $x$ -axis of each graph represents time or frequency, and the  $y$ -axis represents amplitude. The amplitude is measured in volts (V) or decibels (dB). The different combinations of superposition signals have distinct characteristics. In the first row, the superposition frequency difference is 1 Hz, the second row is 0.1 Hz, and the third row is 0.01 Hz.

In the basic FFT result, using the shortest time, 0.1 s cannot distinguish two superposition frequencies with different frequency combinations, as shown in Figure 3a,d,g. Increasing the simulation time influences the signal form so that it is far from the sinusoidal form. Using 50.00 Hz and 52.00 Hz, the basic FFT can distinguish each frequency with longer times, 1 s and 10 s, in Figure 3b,c. When changing the frequency combination to 50.00 Hz and 50.20 Hz, time 1 s cannot recognize the frequencies shown in Figure 3e but can detect two frequencies with longer time 10 s in Figure 3f. For extremely close frequency combinations 50.00 Hz and 50.02 Hz, the graph detected two superposition frequencies as single frequencies in any time setting, as shown in Figure 3g–i. Therefore, the basic FFT is limited in recognizing the superposition of extremely close frequencies that need extended time-domain signals. The longer time means longer computational time to detect the signal frequencies.

### 2.1.2. Short-Time Fourier Transform (STFT)

Another signal analysis method is the Short-Time Fourier Transform (STFT), which uses a time–frequency domain. The application of time–frequency analysis enables the examination of signals in both time and frequency domains, aiding in efficiently identifying signal characteristics across diverse time intervals and frequency bands.

The STFT method presents distinct advantages in signal analysis by breaking down a signal using a short-time window function. One significant benefit of STFT is its capability to capture time-varying characteristics of signals, enabling the examination of transient phenomena and dynamic frequency changes. Unlike the Fast Fourier Transform (FFT) and Discrete Fourier Transform (DFT), which analyze entire signals simultaneously, STFT offers a localized frequency analysis. This localization allows for a more precise examination of frequency components over different time intervals, enhancing the resolution of frequency content in signals with multiple components or rapid changes. Moreover, STFT adapts the window size to accommodate variations in signal characteristics, making it particularly useful for analyzing non-stationary signals. Overall, the STFT method offers a valuable tool for understanding time-varying signals with improved resolution and sensitivity compared to FFT and DFT techniques. The signal transformed by STFT can be defined as [1,35]:

$$w(n) = \begin{cases} 1, & 0 \leq n \leq L_w \\ 0, & \text{else} \end{cases} \quad (3)$$

$$F(f) = \sum_{n=-\infty}^{\infty} x(n)w(n-t)e^{-j2\pi fn} \quad (4)$$

where  $f$  represents the frequency,  $x$  is a signal function,  $n$  is signal sampling,  $w$  is a window function at  $n$  on the time axis,  $L_w$  is window length.

The vibration signal-based STFT algorithm transformed into a time–frequency domain was tried at various times, as well as superposition and sampling frequencies, as shown in Figure 4. The first superposition frequency is 50.00 Hz and 52.00 Hz, the second is 50.00 Hz and 50.20 Hz, and the third is 50.00 Hz and 50.02 Hz, respectively. The simulation superposition frequencies used times 1 s and 10 s at sampling frequency 1000, then were tried in time 10 s at sampling frequency 200. The  $x$ -axis of each graph represents time, which is in seconds, and the  $y$ -axis represents frequency in Hertz.

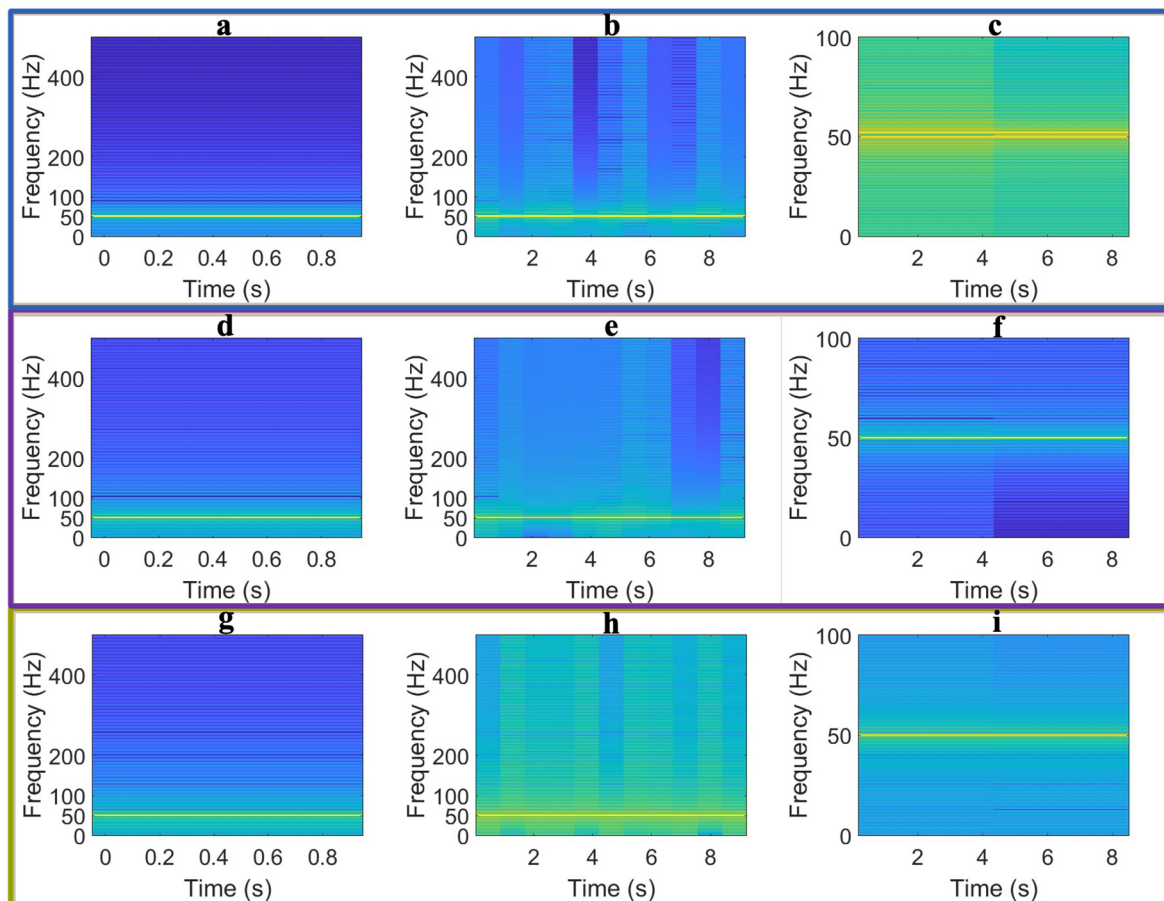


**Figure 4.** Short-Time Fourier Transform (STFT). (a–c) 50.00 + 52.00 Hz with times 1 s, 10 s; (d–f) 50.00 + 50.20 Hz with times 1 s, 10 s; (g–i) 50.00 + 50.02 Hz with times 1 s, 10 s.

In the first row, the superposition frequency difference is 1 Hz, the second row is 0.1 Hz, and the third row is 0.01 Hz. In the STFT result, using times 1 s and 10 s with sampling frequency 1000 and the frequency combination 50.00 Hz and 52.00 Hz cannot distinguish two superposition frequencies, as shown in Figure 4a,b. With a time of 10 s and minimizing the frequency sampling window to 200, STFT can detect the superposition frequency correctly, as depicted in Figure 4c. When changing the frequency combination to 50.00 Hz and 50.20 Hz, times 1 s and 10 s cannot recognize the frequencies shown in Figure 4d–f. For extremely close frequency combinations 50.00 Hz and 50.02 Hz, the graph detected two superposition frequencies as single frequencies in any time setting and sampling frequency window, as shown in Figure 4g–i.

The STFT method, while adequate for many signal analysis tasks, presents limitations in recognizing the superposition of extremely close frequencies. One significant disadvantage lies in the trade-off between time and frequency resolution inherent in the STFT approach. When dealing with closely spaced frequencies, the window size required to

achieve adequate frequency resolution may result in a loss of temporal resolution, making it challenging to distinguish between closely spaced frequency components accurately.

Additionally, the fixed window size in STFT may not be optimal for capturing rapid changes or transient events in signals containing superimposed frequencies. These limitations hinder the ability of STFT to precisely resolve and separate individual frequency components in scenarios involving the superposition of extremely close frequencies.

### 2.1.3. Other Signal Analysis Methods

The other signal analysis methods, such as the time-domain method, employing selected parameters like peak values, RMS (Root Mean Square) or mean values, crest factor, PCA (Principal Component Analysis), and kurtosis for vibration frequency detection, entails scrutinizing signal characteristics directly within the time domain [36]. This approach computes various statistical parameters from the raw vibration signal, including peak values (maximum or minimum amplitude), RMS values (a measure of signal magnitude), mean values (average amplitude), crest factor (peak-value-to-RMS-value ratio), PCA (a method for dimensionality reduction and feature extraction), and kurtosis (a gauge of the shape of the probability distribution of a signal's values). By evaluating these parameters, engineers can glean insights into the overall behavior and attributes of the vibration signal, facilitating the identification of anomalies or patterns indicative of specific mechanical faults or operational conditions. This method proves particularly beneficial for detecting alterations in vibration patterns associated with faults like unbalance, misalignment, bearing defects, or rotor eccentricity in rotating machinery.

Despite its potential, the utilization of the time-domain signal analysis method with selected parameters for vibration frequency detection is relatively limited [37]. Firstly, this method may not consistently capture the complete complexity of vibration signals, particularly when fault signatures are subtle or nonlinear. The selected signal parameters may inadequately represent the underlying characteristics of the vibration signal, resulting in restricted effectiveness for fault detection or diagnosis. Additionally, interpreting these selected parameters often demands significant expertise and experience, as they may not directly elucidate specific fault conditions or mechanical anomalies within the machinery. Engineers may encounter challenges in accurately interpreting results without comprehensively understanding the analyzed system.

Furthermore, reliance on a predefined set of parameters may constrain the method's flexibility and adaptability across various machinery types or fault scenarios. Vibration signals exhibit considerable variability influenced by machine type, operating conditions, and environmental elements, complicating the development of universally applicable parameters for fault detection. While the time-domain signal analysis method utilizing selected parameters offers valuable insights into machinery vibration characteristics, its limited efficacy, interpretability, and adaptability contribute to its comparatively lower adoption than alternative vibration analysis techniques, such as frequency-domain analysis or machine learning-based approaches.

## 3. The Proposed System

Based on Figure 2, TensorFlow, a well-known framework in deep learning, develops a DNN tailored for two-dimensional (2D) vibration signal image classification tasks from a time-domain vibration signal in the sinusoidal waveform. As the vibration signal frequency is converted into 2D image data, the process of vibration signal detection inherently entails a recognition procedure. The system configuration aimed to detect the presence of a Graphics Processing Unit (GPU), optimizing computational efficiency, which is crucial for machine learning training.

The dataset consisted of various MATLAB-generated 2D vibration signal frequencies, classified into fifty-one classes from the data range 0–0.5 with delta 0.01. Both sets of vibration signals are converted into 2D images [10,38], with the simulation data employed for

training DNN. The DNN parameters are shown in Table 1. These datasets are systematically divided into training and validation subsets for training purposes.

**Table 1.** Parameters of the proposed DNN structure.

Layer	Parameters
Number of neurons in the input layer	256*256*3
Number of hidden layers	3
Number of neurons in each layer	Various-128-51
Activation function	ReLU
Optimizer algorithm	Adam
Learning rate	Dynamic
Batch size	32
Number of epochs	100

To meet the model's input specifications, each image was processed to fit the required dimension of  $256 \times 256$  pixels, aligning with the pre-processing requirements of the ResNet50 architecture. These steps are imperative to ensure that the dataset is compatible with the model initially trained on ImageNet. Furthermore, the augmented techniques are applied to the training data, including random rotations, shifts in width and height, and horizontal flipping. These techniques introduced variation and enhanced the robustness of the dataset, simulating a broader array of training scenarios. From the whole dataset, a substantial portion of the dataset is allocated, precisely twenty percent, for validation. This division allowed for a thorough assessment of the model's performance. It enriched the training process by incorporating a diverse set of data samples.

The architecture of the proposed DNN focused on the ResNet50 model, a fifty-layer convolutional neural network pre-trained on the comprehensive ImageNet dataset. This convolutional neural network pre-trained model is utilized mainly for feature extraction of 2D vibration signal images, maintaining its pre-trained weights unchanged to concentrate learning on the layers uniquely relevant to the proposed scheme. The architecture has enhanced the architecture by integrating several layers designed for our classification goals.

These additions included a Global Average Pooling 2D layer, which reduced feature map dimensionality and helped prevent overfitting, a fully connected Dense layer with 128 neurons for learning significant high-level features related to our dataset, and a Dropout layer with a fifty percent rate to introduce regularization, crucial for avoiding overfitting. The architecture culminated in a Dense layer with softmax activation, intended for categorizing input images into one of fifty-one groups.

Selecting the ReLU activation function for the hidden Dense layer was crucial, providing the required nonlinearity for the network to discern complex patterns in the dataset. In the training process, employing an Adam optimizer is carefully managed with an initial learning rate of  $1 \times 10^{-5}$ , subject to dynamic adjustments. This flexible learning rate, regulated by a systematic scheduler, was vital in steering the model towards an effective weight configuration. Various callbacks were applied throughout training to refine the learning process: early stopping mechanisms to prevent excessive training, learning rate modifications for efficient convergence, model checkpointing to preserve the most effective model state, and epoch history recording for insights into training progress. In cases where an existing checkpoint was available, training recommenced from that point, thus avoiding any loss of progress and enhancing training efficiency.

The training process, comprising up to a hundred epochs and a batch size of thirty-two, reached a notable point in this study. The final model, which embodies the detailed patterns and features acquired during training, is carefully preserved.

This model, resulting from an extensive learning process, is now prepared for application in various frequencies of 2D vibration signal image classification tasks.

The proposed method effectively utilizes the potential of pre-trained networks within a transfer learning framework, emphasizing the advantages of using established architectures as foundational elements for additional learning. This approach proves the practicality and flexibility of deep learning techniques in managing image-based datasets. It highlights the importance of fine-tuning to tailor pre-trained models to specific classification requirements. The capability of the proposed model to identify and categorize various frequencies of 2D vibration signal images across fifty-one categories illustrates the adaptability of DNN in extracting and learning from intricate patterns in visual data, setting the stage for novel applications in areas including automated 2D vibration signal image categorization and advanced image-based vibration recognition system.

#### 4. Results and Discussion

This section demonstrates the results of the image-based vibration signal recognizing training loss and accuracy value, as well as the accuracy of the DNN model for single and superposition frequency. The accuracy comparison of using simulation and experiment data for a single frequency is also discussed.

As mentioned in the previous section, the vibration signal neglects the signal noise level. Thus, the simulation of motor vibration, represented using a time-domain sinusoidal waveform, was carried out in MATLAB 2023b with various single-signal frequencies. Without any signal analysis method, these time-domain data must be converted into 2D images before training. The training dataset demonstrates notable performance, attaining high accuracy in image-based vibration signal recognition. Figure 5a–c illustrate the loss and accuracy of the training throughout the DNN model training epochs, which are applied in various frequency ranges such as 50 Hz, 100 Hz, and 500 Hz, respectively.

Three different frequency ranges are chosen based on the electric motor's fundamental (50 or 60 Hz) and harmonic frequencies (odd multiple of the motor's fundamental frequency). These harmonic frequencies indirectly impact the motor's performance. Notably, the presence of harmonics within the motor drive system can adversely affect the power quality of electrical power supplied, potentially leading to severe consequences [39]. The accuracy of both datasets notably improves with DNN model training, signifying the proposed method's effectiveness in enhancing the model's generalization capability. The  $x$ -axis represents the epoch ranging from 0 to 100, the number of times the model has gone through the entire training dataset. The right  $y$ -axis represents the loss value, and the left  $y$ -axis represents the accuracy value, which varies from 0 to 1. The blue line represents the loss of the model. The red line represents the accuracy of the model.

Among various evaluation metrics, accuracy, precision, recall, and F1 score are commonly employed to assess the performance of DNN models. These metrics were utilized to scrutinize the effectiveness of the proposed method during model training. Accuracy assesses the overall correctness of predictions, representing the proportion of correctly classified samples. The accuracy value of different frequency ranges is 95.16% for 50 Hz, 94.2% for 100 Hz, and 93.52% for 500 Hz.

Precision gauges the precision of positive predictions, indicating the proportion of correctly predicted positive samples among all positive predictions. All the precision values have numbers above 90%, as shown in Figure 5a–c. Recall, also referred to as the true positive rate, quantifies the ability to correctly identify positive samples, evaluating the detection capability for true positive samples. The highest recall value is for frequency 500 Hz training. The F1 score, a combined metric, considers both precision and recall, offering a balanced measure of model performance. The highest F1 score value is for frequency 50 Hz training.

The model's accuracy, precision, recall, and F1 score all increase as the number of epochs increases. This means the model is learning and improving its ability to make correct predictions over time.

Overall, the simulation results of the proposed model underscore its promise, demonstrating the capability to recognize a single frequency below 1 Hz with a noteworthy accuracy across diverse frequency ranges.

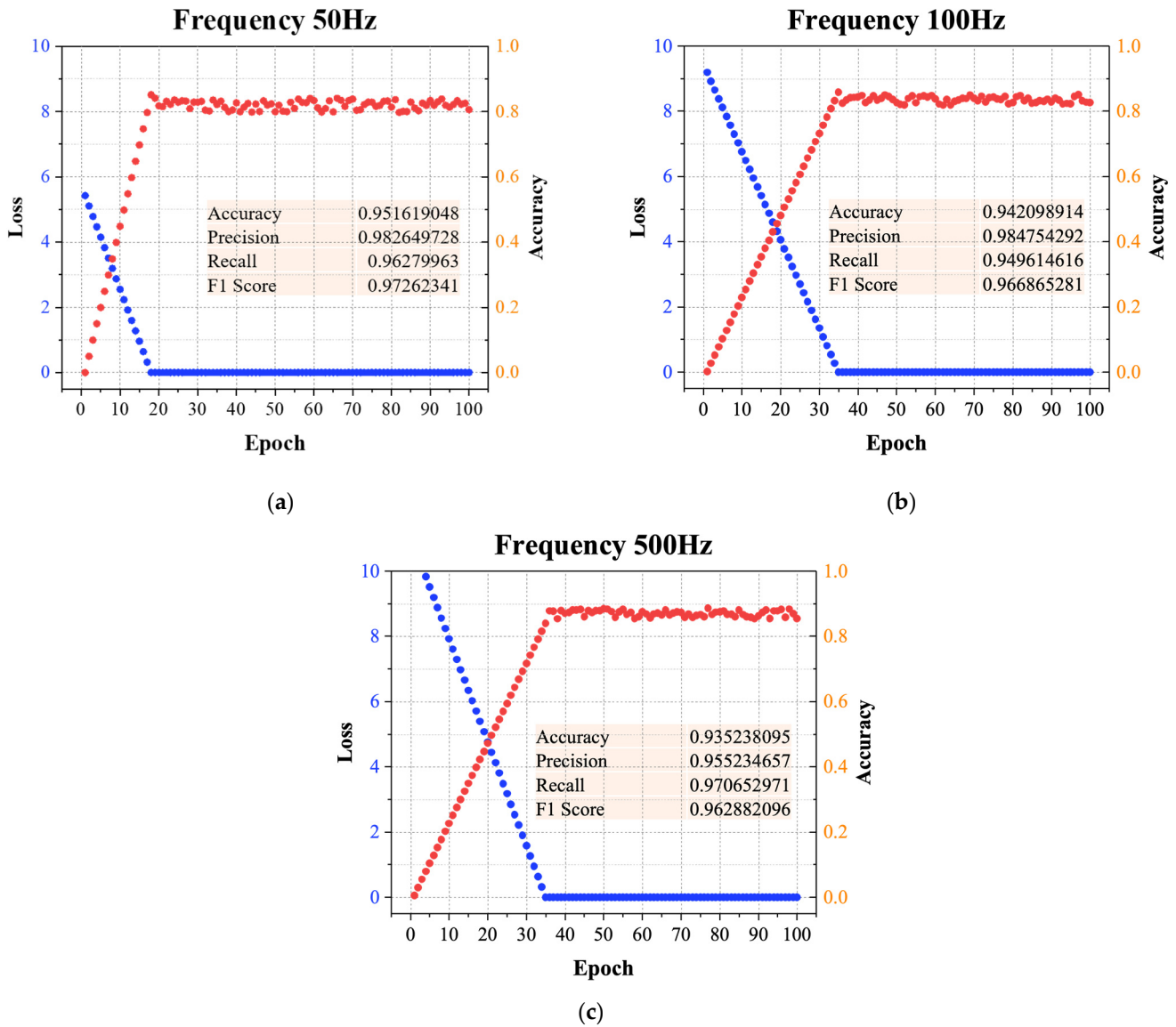


**Figure 5.** The result of frequency detection loss and accuracy in various ranges. (a) Frequency 50 Hz, (b) Frequency 100 Hz, (c) Frequency 500 Hz.

**4.1. Recognize Single Vibration Frequency**

The first proposed system scheme was tested by recognizing specific image-based vibration signals with a single frequency. This recognition process is DNN model testing using simulation data. The frequency-recognized data are the first 11th frequency in the ranges of 50.00–50.50 Hz with a delta of 0.01, as shown in Figure 6. Thus, the frequency-recognized data range is from 50.00 Hz to 50.10 Hz.

The recognition of single vibration frequency is the basic process of multiple or superposition frequency recognition that holds significant importance as it forms the foundational process for identifying multiple or superposition frequencies, especially in motor vibration analysis. Accurately identifying individual vibration frequencies lays the groundwork for understanding more complex vibration patterns and motor behavior.

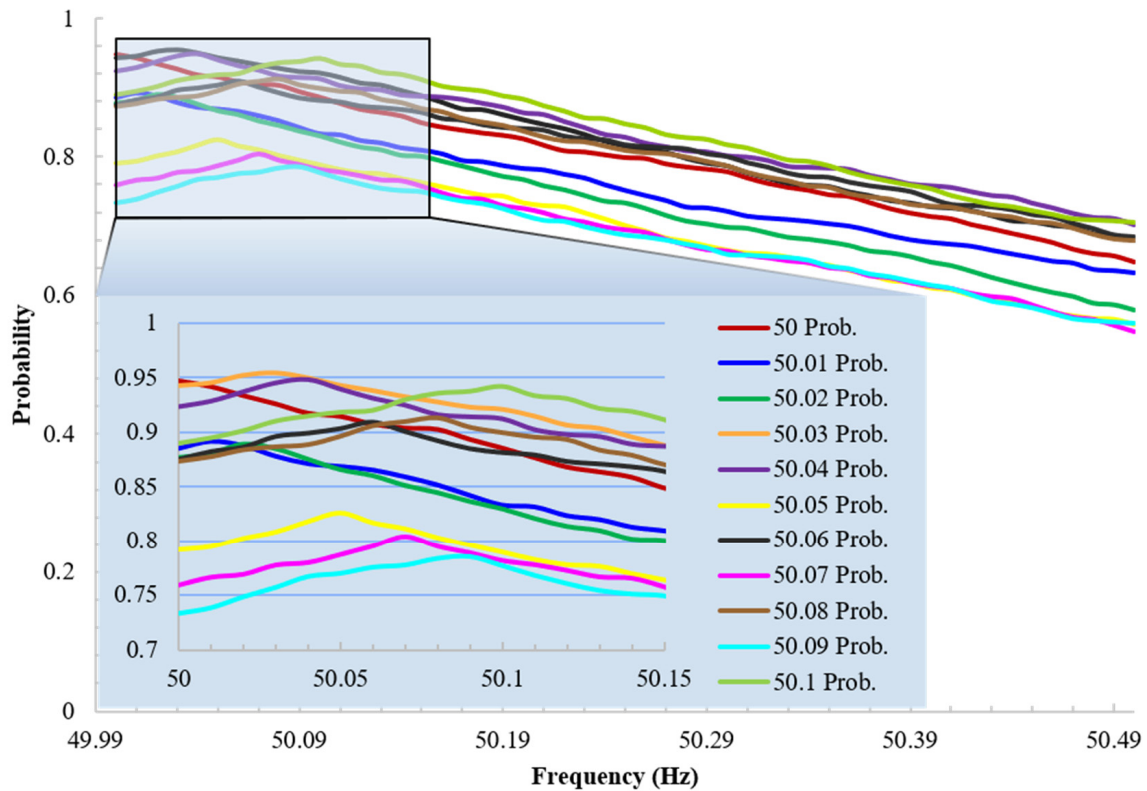


**Figure 6.** The recognition probability for a single frequency using simulation testing data.

It is essential to analyze the resulting probability of each single vibration frequency and then compare it with the superposition frequency to know the performance of the proposed recognition system. The probability value of vibration signal recognition illustrates the frequency recognition accuracy based on the DNN model. The highest accuracy represents the frequency value of the 2D image that can be recognized.

In Figure 6, the *x*-axis represents frequency, and the *y*-axis represents the probability value. As shown in the figure, the proposed system correctly recognizes a single vibration frequency in every frequency between 50.00 Hz and 50.10 Hz. The first red line represents frequency 50.00 Hz, with the recognition probability 0.9474 or 94.74%. The following lines are blue, green, and orange, representing frequencies 50.01 Hz, 50.02 Hz, and 50.03 Hz, with the recognition probability of 89.11%, 88.94%, and 95.36%, respectively. The following line is purple, yellow, and dark grey, representing frequencies 50.04 Hz, 50.05 Hz, and 50.06 Hz, with the recognition probability of 94.81%, 82.54%, and 90.91%, respectively. The last four lines, magenta, brown, sky blue, and light green, represented frequencies 50.07 Hz, 50.08 Hz, 50.09 Hz, and 50.10 Hz, with the recognition probability of 80.37%, 91.29%, 78.54%, and 94.15%.

#### 4.2. Recognize Superposition Vibration Frequency

The second proposed vibration frequency recognition scheme system was tested by recognizing specific image-based vibration signals with a multiple or superposition frequency, which combines two extremely close frequencies between 50.00 Hz and 50.10 Hz, as shown in Figure 7. The frequency-recognized data range is the same as the previous scheme used to analyze the performance by comparing the probability values equally. Due to this scheme consisting of two extremely close frequencies, the frequency recognized is the two of the highest probability values.

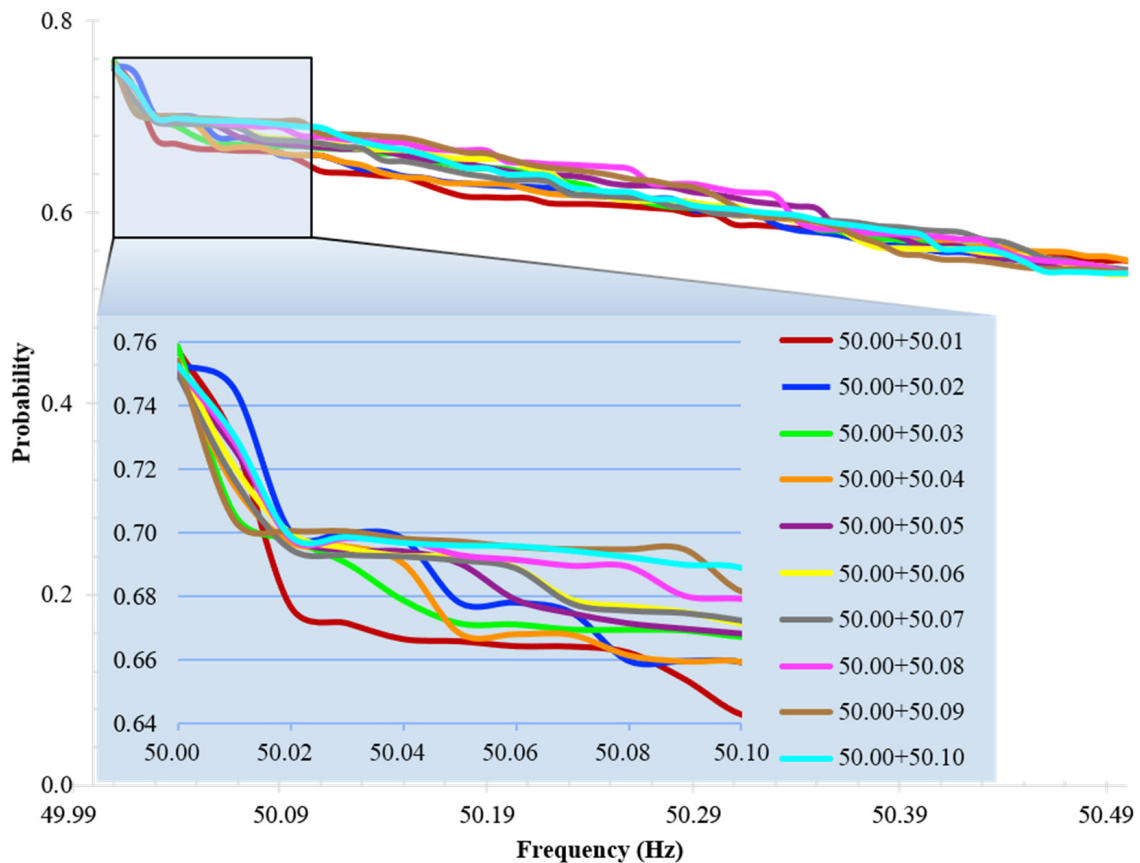


**Figure 7.** The recognition probability for superposition frequency using simulation testing data.

In Figure 7, the  $x$ -axis represents frequency, and the  $y$ -axis represents the probability value. The proposed system correctly recognizes superposition frequency, meaning that each line contains two superposition frequencies. The superposition frequency has one fixed frequency value of 50.00 Hz, and the other has a varied frequency value from 50.01 Hz to 50.10 Hz.

The first red line represents a superposition frequency of 50.00 Hz and 50.01 Hz with a recognition probability of 75.78% and 72.93%, respectively. The following lines are blue, green, and orange, representing frequencies 50.00 + 50.02 Hz, 50.00 + 50.03 Hz, and 50.00 + 50.04 Hz, with the recognition probability of 75.33% and 68.83%, 75.87% and 70.59%, and 75.07% and 71.49%, respectively.

The following line is purple, yellow, and grey, representing frequencies 50.00 + 50.05 Hz, 50.00 + 50.06 Hz, and 50.00 + 50.07 Hz, with the recognition probability of 75.01% and 72.66%, 75.44% and 72.11%, and 75.03% and 58.45%, respectively. The last three lines, magenta, brown, and sky blue, represented frequencies 50.00 + 50.08 Hz, 50.00 + 50.09 Hz, and 50.00 + 50.10 Hz, with the recognition probability of 75.22% and 72.89%, 75.42% and 70.40%, and 75.27% and 73.06%, respectively. The probability varies from 0.7854 to 0.9536, and the line peak value represents the frequency recognized in the  $y$ -axis.

The DNN model correctly recognized eight frequencies from ten frequency combinations based on the superposition frequency result. It influences the true positive (TP), false negative (FN), false positive (FP), and true negative (TN) values. Additionally, the probability value of simulation data using single vibration frequency signals is higher than the probability value of superposition vibration frequency signals.

#### 4.3. Comparison of Simulation and Experimental Motor Vibration Frequency

The subsequent discussion explains the recognition using FBG experiment data and compares the simulation and experimental vibration frequency signal. In Figure 8, the

graph color order is the same as the previous graph in Figure 6. There are various ranges of recognition probability in this figure. The highest probability value is the green line representing frequency 50.02 Hz, with a recognition probability of 70.34%. Using the FBG experiment testing data has a lower recognition probability than simulation data. However, the proposed system correctly recognizes the vibration frequency.

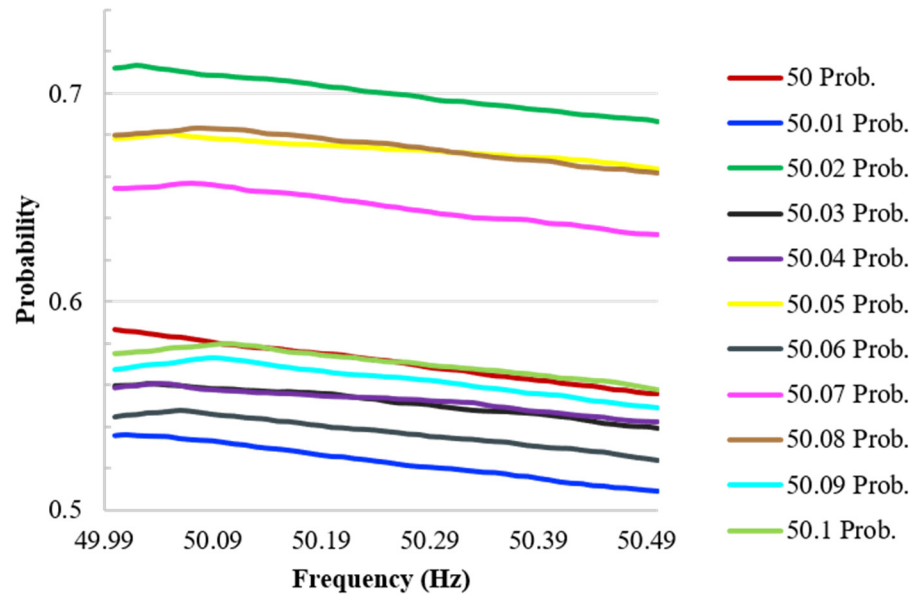


Figure 8. The recognition probability for a single frequency using FBG experiment testing data.

Figure 9 illustrates the comparison of simulation and experimental vibration signal data at a single frequency of 50.02 Hz using the proposed system. The  $x$ -axis represents frequency in Hz, and the  $y$ -axis represents the probability value from 0.5 to 1. Two lines on the graph, red and blue, represent the simulation and experiment results, respectively. Using simulation data, it recognized 50.02 Hz correctly, with the highest probability starting at 0.8893 until the lowest probability of 0.5792 at 50.50 Hz. Using experimental data, it recognized 50.00 Hz correctly, with the highest probability starting at 0.7034 until the lowest probability was 0.6761 at 50.50 Hz.

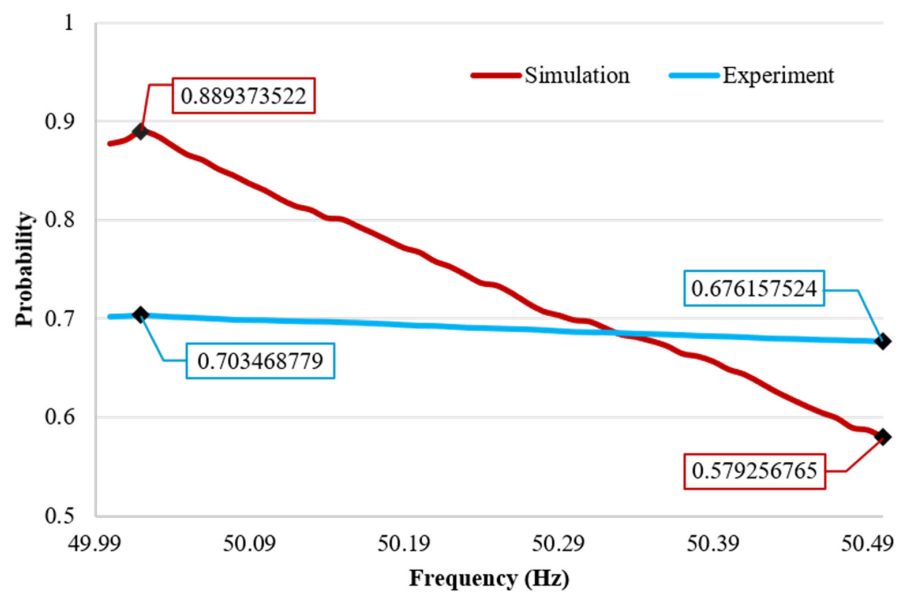


Figure 9. The probability comparison for a single frequency between simulation and experiment data.

Based on Figure 9, the simulation data results have a more comprehensive range of probability than the experimental data in terms of recognizing the single frequency across the given range. The tendency for simulation data to exhibit more linearity than experimental data can be attributed to several factors. Simulations, often reliant on simplified models of intricate systems, tend to overlook the complexities inherent in real-world phenomena. These simplified models may impose constraints and assumptions that lead to more linear outcomes.

Additionally, simulations typically operate in idealized conditions, free from measurement errors inherent in experimental setups. This absence of real-world disturbances can contribute to the perceived linearity of simulation data. Furthermore, the process of parameterization in simulations, wherein parameters are adjusted to fit specific conditions, may inadvertently introduce linearity into the results.

The proposed system has yielded a DNN model trained using only single simulation data, yet it demonstrates the ability to recognize both single and superposition simulation signals, as well as single experimental signals. This capability significantly enhances the system's versatility, as it increases the likelihood of accurately identifying any combination of multiple or superposition signals, whether they originate from simulations or experimental measurements.

Training the DNN model with the simulation data has effectively developed a robust framework capable of handling various signal compositions and complexities. This adaptability ensures the system's effectiveness in real-world scenarios, where signals may exhibit diverse characteristics and combinations. Overall, the proposed system's ability to recognize both single and superposition signals from simulations and experiments marks a significant advancement in signal recognition methodologies.

## 5. Conclusions

This study discusses the new novel extremely close vibration frequency signal recognition system using image-based DNN. Comparative analysis with traditional signal analysis methods, such as Fast Fourier Transform (FFT) and Short-Time Fourier Transform (STFT), was conducted using identical signals. Surprisingly, the results revealed inaccuracies in vibration frequency detection by FFT and STFT methods at specific times, highlighting the limitations of these conventional approaches.

Key findings from the analysis include:

- Simulation results showcase the remarkable accuracy and confirm the expectations of the proposed DNN model, achieving an impressive validation accuracy of 95.16%.
- The ability of the proposed system to discern extremely close frequency vibrations using an unmodified Fiber Bragg Grating (FBG) sensor demonstrates its high sensitivity and precision.
- Extensive testing data utilized by the proposed system enabled accurate identification of both single and superposition vibration frequency signals without relying on signal analysis methods.
- Utilizing a simple and cost-effective FBG experimental setup employing a single FBG further enhances the practicality and accessibility of the proposed system for vibration frequency detection.

Moreover, the proposed system exhibits potential applicability across diverse vibration sensors and sources, capable of handling complex superposition vibration frequency signals with or without noise. This underscores the versatility and robustness of the proposed system approach in addressing various vibration monitoring needs across different engineering applications.

**Author Contributions:** Conceptualization: M.P.J., C.-K.Y. and P.-C.P.; methodology: M.P.J. and P.-C.P.; data preparation: M.P.J., M.I.L. and P.-C.P.; software: M.P.J., M.I.L. and P.-C.P.; model validation: M.P.J., M.I.L. and P.-C.P.; formal analysis: M.P.J., Y.C.M., A.M.D. and P.-C.P.; investigation: M.P.J., C.-K.Y., A.M.D., Y.C.M. and P.-C.P. All authors have read and agreed to the published version of the manuscript.

**Funding:** This work was supported by the National Science and Technology Council, Taiwan, under Grant NSTC 112-2221-E-027-076-MY2.

**Institutional Review Board Statement:** Not applicable.

**Informed Consent Statement:** Not applicable.

**Data Availability Statement:** The data presented in this study are available in this article.

**Conflicts of Interest:** The authors declare no conflicts of interest.

### Abbreviations

The following abbreviations are used in this manuscript:

CNN	Convolutional Neural Networks
DFT	Discrete Fourier Transform
DNN	Deep Neural Networks
DP	Displacement Platform
FBG	Fiber Bragg Grating
FFT	Fast Fourier Transform
FN	False Negative
FP	False Positive
GPU	Graphics Processing Unit
M	Motor
OC	Optical Circulator
OSC	Oscilloscope
PC	Personal Computer
PCA	Principal Component Analysis
PD	Photodetector
PID	Proportional Integral Derivative
ReLU	Rectified Linear Unit
RMS	Root Mean Square
S	Sensor
SG	Signal Generator
STFT	Short-Time Fourier Transform
SVM	Support Vector Machine
TL	Tunable Laser
TN	True Negative
TP	True Positive
VG	Vibration Generator
XGBoost	Extreme Gradient Boosting
YOLO	You Only Look Once
2D	Two-Dimensional

### References

1. Yang, N.-C.; Yang, J.-M. Fault Classification in Distribution Systems Using Deep Learning with Data Preprocessing Methods Based on Fast Dynamic Time Warping and Short-Time Fourier Transform. *IEEE Access* **2023**, *11*, 63612–63622. [[CrossRef](#)]
2. Lu, S.; Qian, G.; He, Q.; Liu, F.; Liu, Y.; Wang, Q. In Situ Motor Fault Diagnosis Using Enhanced Convolutional Neural Network in an Embedded System. *IEEE Sens. J.* **2020**, *20*, 8287–8296. [[CrossRef](#)]
3. Xu, Y.; Yan, X.; Sun, B.; Liu, Z. Deep Coupled Visual Perceptual Networks for Motor Fault Diagnosis under Nonstationary Conditions. *IEEE/ASME Trans. Mechatron.* **2022**, *27*, 4840–4850. [[CrossRef](#)]
4. Samanta, A.K.; Routray, A.; Khare, S.R.; Naha, A. Minimum Distance-Based Detection of Incipient Induction Motor Faults Using Rayleigh Quotient Spectrum of Conditioned Vibration Signal. *IEEE Trans. Instrum. Meas.* **2021**, *70*, 3508311. [[CrossRef](#)]
5. Wang, Y.; Zheng, L.; Gao, Y.; Li, S. Vibration Signal Extraction Based on FFT and Least Square Method. *IEEE Access* **2020**, *8*, 224092–224107. [[CrossRef](#)]

6. Linessio, R.P.; Sousa, K.d.M.; da Silva, T.; Bavastri, C.A.; Antunes, P.F.d.C.; da Silva, J.C.C. Induction Motors Vibration Monitoring Using a Biaxial Optical Fiber Accelerometer. *IEEE Sens. J.* **2016**, *16*, 8075–8082. [[CrossRef](#)]
7. Puche-Panadero, R.; Martinez-Roman, J.; Sapena-Bano, A.; Burriel-Valencia, J.; Pineda-Sanchez, M.; Perez-Cruz, J.; Riera-Guasp, M. New Method for Spectral Leakage Reduction in the FFT of Stator Currents: Application to the Diagnosis of Bar Breakages in Cage Motors Working at Very Low Slip. *IEEE Trans. Instrum. Meas.* **2021**, *70*, 3056741. [[CrossRef](#)]
8. Henry, M. An ultra-precise Fast Fourier Transform. *Meas. Sens.* **2024**, *32*, 101039. [[CrossRef](#)]
9. Sun, S.; Liu, Y.; Eldean, M.A.S. Design and implementation of an optical fiber sensing based vibration monitoring system. *J. Vibroengineering* **2021**, *23*, 496–511. [[CrossRef](#)]
10. Mayaki, M.Z.A.; Riveill, M. Machinery Anomaly Detection using artificial neural networks and signature feature extraction. In Proceedings of the 2023 International Joint Conference on Neural Networks (IJCNN), Gold Coast, Australia, 18–23 June 2023; pp. 1–10. [[CrossRef](#)]
11. Bensaoucha, S.; Moreau, S.; Bessedik, S.A.; Ameer, A. Broken Rotor Bars Fault Detection in Induction Machine Using Machine Learning Algorithms. In Proceedings of the 2022 19th IEEE International Multi-Conference on Systems, Signals and Devices, SSD 2022, Sétif, Algeria, 6–10 May 2022; Institute of Electrical and Electronics Engineers Inc.: Sétif, Algeria, 2022; pp. 851–856. [[CrossRef](#)]
12. Yao, C.-K.; Manie, Y.C.; Peng, P.-C. Free Space Optical Communication for Vibration Sensing of Multiple-Channel Fiber Bragg Grating Array. In Proceedings of the Advanced Photonics Congress 2023, Busan, Republic of Korea, 9–13 July 2023.
13. Amorebieta, J.; Ortega-Gomez, A.; Durana, G.; Fernández, R.; Antonio-Lopez, E.; Schülzgen, A.; Zubia, J.; Amezcua-Correa, R.; Villatoro, J. Highly sensitive multicore fiber accelerometer for low frequency vibration sensing. *Sci. Rep.* **2020**, *10*, 16180. [[CrossRef](#)]
14. Li, Y.; Chen, F.; Guo, T.; Wang, R.; Qiao, X. Sensitivity Enhancement of Fiber Bragg Grating Accelerometer Based on Short Grating. *IEEE Trans. Instrum. Meas.* **2022**, *71*, 3126848. [[CrossRef](#)]
15. Wang, J.; Wei, L.; Li, R.; Liu, Q.; Yu, L.; Li, T.; Tan, Y. An FBG-based 2-D vibration sensor with adjustable sensitivity. *IEEE Sens. J.* **2017**, *17*, 4716–4724. [[CrossRef](#)]
16. de Pelegrin, J.; Dreyer, U.J.; Sousa, K.M.; da Silva, J.C.C. Smart Carbon-Fiber Reinforced Polymer Optical Fiber Bragg Grating for Monitoring Fault Detection in Bearing. *IEEE Sens. J.* **2022**, *22*, 12921–12929. [[CrossRef](#)]
17. Guo, T.; Zhang, T.; Li, Y.; Qiao, X. Highly Sensitive FBG Seismometer with a 3D-Printed Hexagonal Configuration. *J. Light. Technol.* **2020**, *38*, 4588–4595. [[CrossRef](#)]
18. Brusamarello, B.; da Silva, J.C.C.; Sousa, K.d.M.; Guarneri, G.A. Bearing Fault Detection in Three-Phase Induction Motors Using Support Vector Machine and Fiber Bragg Grating. *IEEE Sens. J.* **2022**, *23*, 4413–4421. [[CrossRef](#)]
19. Dejbani, E.; Manie, Y.C.; Deng, Y.-J.; Bitew, M.A.; Tan, T.-H.; Peng, P.-C. High Accuracy and Cost-Effective Fiber Optic Liquid Level Sensing System Based on Deep Neural Network. *Sensors* **2023**, *23*, 2360. [[CrossRef](#)]
20. Ding, M.; Zhang, T.; Wang, R.; Su, D.; Qiao, X. A Low-Flow Fiber-Optic Flowmeter Based on Bending Measuring Using a Cladding Fiber Bragg Grating. *IEEE Sens. J.* **2023**, *23*, 3609–3614. [[CrossRef](#)]
21. Yao, C.-K.; Lin, T.-C.; Chen, H.-M.; Hsu, W.-Y.; Manie, Y.C.; Peng, P.-C. Inclination Measurement Adopting Raman Distributed Temperature Sensor. *IEEE Sens. J.* **2023**, *23*, 22543–22555. [[CrossRef](#)]
22. Mohammed, A.; Djurovic, S. Electric Machine Bearing Health Monitoring and Ball Fault Detection by Simultaneous Thermo-Mechanical Fibre Optic Sensing. *IEEE Trans. Energy Convers.* **2021**, *36*, 71–80. [[CrossRef](#)]
23. Xu, B.; Zhang, X.; Jiang, J.; Liu, K.; Wang, S.; Fan, X.; Jiang, L.; Li, Y.; Chu, Y.; Liu, T. Method of damage location determination based on a neural network using a single Fiber Bragg Grating sensor. *Appl. Opt.* **2019**, *58*, 7251–7257. [[CrossRef](#)]
24. Gui, X.; Li, Z.; Fu, X.; Guo, H.; Wang, Y.; Wang, C.; Wang, J.; Jiang, D. Distributed Optical Fiber Sensing and Applications Based on Large-Scale Fiber Bragg Grating Array: Review. *J. Light. Technol.* **2023**, *41*, 4187–4200. [[CrossRef](#)]
25. Li, T.; Guo, J.; Tan, Y.; Zhou, Z. Recent Advances and Tendency in Fiber Bragg Grating-Based Vibration Sensor: A Review. *IEEE Sens. J.* **2020**, *20*, 12074–12087. [[CrossRef](#)]
26. Wu, H.; Chen, J.; Liu, X.; Xiao, Y.; Wang, M.; Zheng, Y.; Rao, Y. One-Dimensional CNN-Based Intelligent Recognition of Vibrations in Pipeline Monitoring with DAS. *J. Light. Technol.* **2019**, *37*, 4359–4366. [[CrossRef](#)]
27. Ruan, S.; Mo, J.; Xu, L.; Zhou, G.; Liu, Y.; Zhang, X. Use AF-CNN for End-to-End Fiber Vibration Signal Recognition. *IEEE Access* **2021**, *9*, 6713–6720. [[CrossRef](#)]
28. Yu, L.; Guo, Q.; Wang, R.; Shi, M.; Yan, F.; Wang, R. Dynamic Offloading Loading Optimization in Distributed Fault Diagnosis System with Deep Reinforcement Learning Approach. *Appl. Sci.* **2023**, *13*, 4096. [[CrossRef](#)]
29. Fouda, B.M.T.; Yang, B.; Han, D.; An, B. Pattern Recognition of Optical Fiber Vibration Signal of the Submarine Cable for Its Safety. *IEEE Sens. J.* **2021**, *21*, 6510–6519. [[CrossRef](#)]
30. Tang, R.; Qin, C.; Zhao, M.; Xu, S.; Tao, J.; Liu, C. An Optimized Fractional-Order PID Horizontal Vibration Control Approach for a High-Speed Elevator. *Appl. Sci.* **2023**, *13*, 7314. [[CrossRef](#)]
31. Kumar, P.; Shih, G.-L.; Yao, C.-K.; Hayle, S.T.; Manie, Y.C.; Peng, P.-C. Intelligent Vibration Monitoring System for Smart Industry Utilizing Optical Fiber Sensor Combined with Machine Learning. *Electronics* **2023**, *12*, 4302. [[CrossRef](#)]
32. Meng, H.; Wang, S.; Gao, C.; Liu, F. Research on Recognition Method of Railway Perimeter Intrusions Based on  $\Phi$ -OTDR Optical Fiber Sensing Technology. *IEEE Sens. J.* **2021**, *21*, 9852–9859. [[CrossRef](#)]
33. Yao, C.K.; Lee, M.C.; Peng, P.C. A Fiber Bragg Grating Sensing System using Tunable Demodulator. In Proceedings of the 2022 IEEE International Conference on Consumer Electronics-Taiwan (ICCE-TW), Beitou, Taipei, Taiwan, 6–8 July 2022.

34. Wu, H.; Lu, H.; Yang, S.; Wang, Y.; Wang, C.; Rao, Y. Vertical offset-distance estimation and threat level prediction of vibrations with DAS. *IEEE Access* **2020**, *8*, 177245–177254. [[CrossRef](#)]
35. Pang, Y.-N.; Liu, B.; Liu, J.; Wan, S.P.; Wu, T.; He, X.-D.; Yuan, J.; Zhou, X.; Long, K.; Wu, Q. Wearable optical fiber sensor based on a bend singlemode-multimode-singlemode fiber structure for respiration monitoring. *IEEE Sens. J.* **2021**, *21*, 4610–4617. [[CrossRef](#)]
36. Orłowska-Kowalska, T.; Wolkiewicz, M.; Pietrzak, P.; Skowron, M.; Ewert, P.; Tarchala, G.; Krzysztofiak, M.; Kowalski, C.T. Fault Diagnosis and Fault-Tolerant Control of PMSM Drives—State of the Art and Future Challenges. *IEEE Access* **2022**, *10*, 59979–60024. [[CrossRef](#)]
37. Liu, D.; Cui, L.; Wang, H. Rotating Machinery Fault Diagnosis Under Time-Varying Speeds: A Review. *IEEE Sens. J.* **2023**, *23*, 29969–29990. [[CrossRef](#)]
38. Liang, P.; Deng, C.; Wu, J.; Yang, Z.; Zhu, J. Intelligent Fault Diagnosis of Rolling Element Bearing Based on Convolutional Neural Network and Frequency Spectrograms. In Proceedings of the 2019 IEEE International Conference on Prognostics and Health Management (ICPHM), San Francisco, CA, USA, 17–20 June 2019.
39. Jati, M.P.; Purwanto, E.; Sumantri, B.; Rusli, M.R.; Nasuha, A.; Tjahjono, A.; Taufik, T. A fuzzy supervisory scalar control for matrix converter induction motor drives. *Int. J. Electr. Eng. Inform.* **2021**, *13*, 203–217. [[CrossRef](#)]

**Disclaimer/Publisher’s Note:** The statements, opinions and data contained in all publications are solely those of the individual author(s) and contributor(s) and not of MDPI and/or the editor(s). MDPI and/or the editor(s) disclaim responsibility for any injury to people or property resulting from any ideas, methods, instructions or products referred to in the content.